



Activated carbon from avocado seeds for the removal of phenolic compounds from aqueous solutions

Anderson J.B. Leite^a, Carmalin Sophia A.^b, Pascal S. Thue^a, Glaydson S. dos Reis^a, Silvio L.P. Dias^a, Eder C. Lima^{a,*}, Julio C.P. Vaghetti^a, Flavio A. Pavan^c, Wagner Soares de Alencar^{a,d}

^aInstitute of Chemistry, Federal University of Rio Grande do Sul (UFRGS), Av. Bento Gonçalves 9500, P.O. Box 15003, 91501-970, Porto Alegre, RS, Brazil, Tel./Fax +55 (51) 3308 7175; emails: profederlima@gmail.com, eder.lima@ufrgs.br (E.C. Lima), barcellos2903@gmail.com (A.J.B. Leite), pascalsilasthue@gmail.com (P.S. Thue), glaydsonambiental@gmail.com (G.S. dos Reis), silvio.dias@ufrgs.br (S.L.P. Dias), juliovaghetti@gmail.com (J.C.P. Vaghetti), drwsa@yahoo.com.br (W.S. de Alencar)

^bNational Environmental Engineering Research Institute (NEERI), Chennai Zonal Laboratory, CSIR Campus, Taramani, Chennai 600113, India, email: ac_sophia@neeri.res.in

^cFederal University of Pampa, UNIPAMPA, Bagé, RS, Brazil, email: flavio.pavan@unipampa.edu.br (F.A. Pavan)

^dInstitute of Exact Sciences, Federal University of South and Southeast of Pará (UNIFESSPA), Marabá, PA, Brazil

Received 11 July 2016; Accepted 27 January 2017

ABSTRACT

Avocado seed activated carbon (ASAC) was synthesized by microwave-heating process using $ZnCl_2$ as an activating agent. The adsorbent ASAC was characterized using analytical techniques namely N_2 isotherms, Fourier transform infrared spectroscopy, and scanning electron microscopy. The surface area of ASAC was $1,432 \text{ m}^2 \text{ g}^{-1}$. The ASAC prepared was used for adsorption of resorcinol and 3-aminophenol from aqueous solutions. Kinetic models namely pseudo-first order, pseudo-second order, and Avrami fractional order and isotherms (Freundlich, Langmuir, and Liu) were applied to the experimental adsorption data. The results demonstrate maximum adsorption capacity for resorcinol (406.9 mg g^{-1}) and 3-aminophenol (454.5 mg g^{-1}) at 50°C . The thermodynamic analysis of data and the effect of temperature studies revealed that the adsorption processes of resorcinol and 3-aminophenol onto ASAC were temperature dependent. The adsorption processes were exothermic and spontaneous. The avocado carbon displayed excellent adsorption properties for the simulated effluents containing phenolic compounds.

Keywords: Avocado seed; Microwave-assisted pyrolysis; Activated carbons; Phenolic compounds; Isotherm and kinetic models; Adsorption

1. Introduction

Water pollution due to phenolic compounds has caused increasing environmental concerns in the last decades [1,2]. Numerous industries such as gas and coke plant's resins, paper and pulp, plywood, paints, pharmaceutical, petroleum, textile, plastic, etc., discharge wastewaters containing different types of phenolic contaminants [1,2]. Phenolic

wastewaters are known to be toxic and carcinogenic. Hence, there is a growing awareness about the impact of these contaminants on water resource.

Phenolic compounds rapidly phototransform and form subproducts that may pose severe risks to aquatic organisms and human beings [1,2]. Ingestion of water contaminated with phenols may cause serious gastrointestinal damages, muscle tremors, difficulty in walking, and death in animals [1,2]. Due to the high environmental risks involved and toxicity of the effluents, it is important

* Corresponding author.

to remove phenol and phenolic compounds from contaminated industrial aqueous streams before being discharged into any water bodies [1,2].

Various treatment processes used for the removal of phenols from water and/or wastewaters are membrane separation [3], advanced oxidation process [4,5], electrochemical oxidation [6], biological processes [7,8], microfiltration and nanofiltration [9,10], and adsorption [11–13]. These chemical, biological, and physical treatment processes have their own advantages and disadvantages. The methods have found limited application, as they are either complex and/or not economical. However, adsorption has been found to be the most attractive method for removal of organic pollutants. The advantage with adsorption is: (i) the method is simple, (ii) adsorbents are reusable, and (iii) the process is highly economical [11–14].

Recently, several materials have been used as adsorbents or as precursors for preparation of adsorbents. Such materials include carbon nanotubes [15], silica [16] and polysiloxanes [17], zeolite [18], sewage sludge [17,19] and tannery sludge [20], and agroindustrial wastes such as *Punica granatum* husk [21], wood sawdust [22,23], Brazilian pine-fruit shell [24], oak shell [25], cocoa shell [26], etc. However, there is always a quest to find new materials with higher adsorption capacity so as to remove a spectrum of highly toxic pollutants from aqueous systems.

Due to textural properties, especially pore volume and specific surface area, activated carbons are widely used for the adsorption of organic pollutants from aqueous solutions [19,20,22–26]. Activated carbons may be prepared by pyrolysis using conventional thermal pyrolysis or microwave-assisted process [22,24]. The main difference among the methods is how the heat is generated. Microwave provides energy directly on the carbon bed [20,22,23] while conventional heating uses conduction and/or convection [24]. Microwave heating is advantageous over conventional pyrolysis, reason being its shorter pyrolysis time (<10 min) [20,26]. As a result, there is rapid temperature rise [20,26], and a remarkable decrease in energy consumption [20].

The main advantage and novelty of present study is that the microwave-induced activated carbons were prepared through a single stage of pyrolysis. The biomass impregnated with inorganics can only be carbonized in a microwave [23]. This is the main reason why researchers carbonize the organic precursors in a conventional furnace to produce carbonized material (i.e., microwave conductor), and subsequently, activated it through microwave induction [27–29]. On the other hand, in the present study, impregnation of the carbon material with inorganics is carried out before microwave-assisted pyrolysis. This task can be established in a single step [20,22,23,26]. This single step process reduces the total time for producing the activated carbons. Another novelty and advantage of this work is that, the total time of pyrolysis including the time for cooling down the quartz reactor was <11 min.

Therefore, the present study aims at the preparation and characterization of activated carbon from avocado seed (ASAC) by microwave-heating process. The prepared avocado shell carbon has been tried as an adsorbent for the removal of phenolics such as resorcinol (RES) and 3-aminophenol (AMP) from aqueous solutions.

2. Experimental

2.1. Chemicals and reagents

The adsorbate RES and AMP (Supplementary Figs. 1 and 2, respectively) were supplied by Vetec (Rio de Janeiro, Brazil). The ZnCl_2 was purchased from Synth (Diadema, SP, Brazil).

Reagents such as RES, AMP, 2-nitrophenol, 2-naphthol, 2-chlorophenol, 4-nitrophenol, hydroquinone, 3-cresol, bisphenol A, phenol, 2-cresol, humic acid, sodium sulfate, sodium chloride, potassium phosphate, sodium carbonate, potassium nitrate were used for the preparation of simulated effluents. All these reagents were supplied by Vetec (Rio de Janeiro, Brazil). 1.0 mol L^{-1} HCl and/or NaOH (Neon, São Paulo, Brazil) were used for pH adjustments.

2.2. Preparation of adsorbents

100.0 g of ZnCl_2 was weighed and dissolved in 50.0 mL of deionized water. 100.0 g of dried avocado seed (AS; milled at diameter < 250 μm) was added to the ZnCl_2 solution and mixed continuously at approximately 80°C for 30 min. After mixing, the paste was dried in an air oven at 90°C for 120 min. Pyrolysis of the AS (10.0 g) impregnated with ZnCl_2 was carried out in a quartz reactor as described elsewhere [20,22,23], under a nitrogen atmosphere (150 mL min^{-1}). The quartz reactor was placed in the microwave oven and the sample was carbonized in four cycles of 80 s at 1,200 W. Then, the system was cooled after pyrolysis for 5 min under 60 mL min^{-1} N_2 . One pyrolysis cycle took <11 min, including 5 min of cooling time. Subsequently, other pyrolysis cycles were carried out.

10.0 g of pyrolyzed carbonaceous material was mixed with 200 mL of 6 mol L^{-1} HCl in a 500 mL boiling flask. The mixture was continuously stirred on a magnetic stirrer and refluxed for 2 h (70°C–80°C). The resultant slurry was cooled down to room temperature and filtered under vacuum using 0.45 μm membrane using a polycarbonate Sartorius system. The filtrate was discarded and the solid material was washed repeatedly until neutral pH with deionized water. Later, the solid material was again mixed with 200 mL of 0.010 mol L^{-1} Ethylenediaminetetraacetic acid (EDTA) (pH 10.0) solution and stirred for 15 min. The solid material was again filtered under vacuum, washed with 100 mL of 0.010 mol L^{-1} EDTA (pH 10.0) to eliminate trace heavy metals from the carbonaceous material. The solid material was again repeatedly washed with deionized water until neutral pH. The resultant carbon was oven dried at 105°C for 5 h, milled to particle sizes $\leq 106 \mu\text{m}$ and stored properly until use. The adsorbent was named as ASAC [20,22,26].

To check the leaching of Zn from the activated carbon prepared, 30.0 mg of ASAC was mixed with 20.0 mL of water in a 50.0 mL Falcon tube and stirred for 24 h. The solid phase was separated by centrifugation, and the liquid phase was analyzed in an Analyst 200 Flame Atomic Absorption Spectrometry – PerkinElmer (Massachusetts, USA) using air-acetylene flame (10:2.5 L min^{-1}). Hollow cathode lamp of Zn ($\lambda = 213.86 \text{ nm}$) of the same manufacturer was used as radiation source.

2.3. Characterization of adsorbent materials

Several analytical techniques were used to understand how the microwave-heating process and the leaching out affected the structure of raw AS and ASAC. The surface

morphologies of ASAC were evaluated by employing a scanning electron microscope (JEOL microscope, model JSM 6060) [23]. The porous structure parameters of ASAC were determined through nitrogen adsorption/desorption isotherms by using a surface area analyzer (Micromeritics Instrument, TriStar II 3020, USA) [23]. The surface functional groups of AS and ASAC were characterized using a Fourier transform infrared spectroscopy (FTIR; Bruker, model alpha, USA) [22].

2.4. Adsorption studies

The adsorption experiments were performed to evaluate the adsorption capacity of ASAC. The concentration of RES and AMP was varied between 100.00–1,800.0 mg L⁻¹. Aliquots of 20.00 mL of adsorbate were taken in 50.0 mL flat Falcon tubes containing 5.0–200.0 mg of ASAC at varying pH conditions (2.0–10.0). The tubes were then capped and placed horizontally in an acclimatized agitator. The samples were agitated for 1–480 min at varied temperature (25°C–50°C).

The samples after a fixed time of agitation were centrifuged using a Unicen M Herolab centrifuge to separate the adsorbent. 1–5 mL of the supernatant was then diluted to 10.0–50.0 mL in standard flasks using the blank solution at suitable pH. The concentration of the unadsorbed RES and AMP was analyzed using a spectrophotometer (T90+ PG Instruments) at wavelengths 273 and 282 nm, respectively.

The sorption capacity and the percentage removal of phenolic compounds are given by Eqs. (1) and (2), respectively:

$$q = \frac{(C_0 - C_f)}{m} \cdot V \quad (1)$$

$$\% \text{Removal} = 100 \cdot \frac{(C_0 - C_f)}{C_0} \quad (2)$$

where q is the sorption capacity of phenolic compounds adsorbed (mg g⁻¹); C_0 is the initial adsorbate concentration (mg L⁻¹); C_f is the adsorbate concentrations in equilibrium (mg L⁻¹); m is the weight of ASAC (g); and V is the volume of the adsorbate in solution (L).

2.5. Statistical evaluation and quality assurance

The experiments were performed in triplicates to assure precision, accuracy, and reliability of data. Blank runs were conducted in parallel [30].

RES and AMP solutions were stored in amber colored glass bottles. All the glassware used in the experiment were precleaned using 10% HNO₃ [31], rinsed with deionized water, dried, and stored in closed cabinets.

Standard calibration graphs of RES and AMP (10.0–150.0 mg L⁻¹) were prepared using UV-Win software of T90+ PG Instruments spectrophotometer. Triplicate analytical analysis was performed, and the precision was maintained ($n = 3$). The detection limits of RES and AMP were 0.013 and 0.011 mg L⁻¹, respectively. The signal/noise ratio was

3 [32]. A spiked phenol solution (70.0 mg L⁻¹) was used as quality control at every 10 determinations. This determined that the readings of the RES and AMP concentrations were accurate [33].

Microcal Origin 2015 application was used to evaluate the best fitting equilibrium and kinetic data, by simplex method and the Levenberg–Marquardt algorithm applying nonlinear equations. The suitability of the equilibrium and kinetic models was evaluated using determination coefficient (R^2), the adjusted determination coefficient (R^2_{adj}), and standard deviation (SD) of residues [34]. The difference between the theoretical and experimental quantities of RES and AMP adsorbed by ASAC was measured using SD. The mathematical expression for R^2 , R^2_{adj} and SD are given by Eqs. (3), (4), and (5), respectively.

$$R^2 = \left(\frac{\sum_i^n (q_{i,\text{exp}} - \bar{q}_{\text{exp}})^2 - \sum_i^n (q_{i,\text{exp}} - q_{i,\text{model}})^2}{\sum_i^n (q_{i,\text{exp}} - \bar{q}_{\text{exp}})^2} \right) \quad (3)$$

$$R^2_{\text{adj}} = 1 - (1 - R^2) \cdot \left(\frac{n - 1}{n - p - 1} \right) \quad (4)$$

$$SD = \sqrt{\left(\frac{1}{n - p} \right) \cdot \sum_i^n (q_{i,\text{exp}} - q_{i,\text{model}})^2} \quad (5)$$

where $q_{i,\text{exp}}$ is the distinct experimental q value; \bar{q}_{exp} represents the mean experimental q values; $q_{i,\text{model}}$ is the distinct theoretical q value predicted by the model; n is the number of experiments; p is the number of variables in the model [34].

2.6. Kinetics of adsorption

Pseudo-first order, pseudo-second order, and Avrami fractional order models were used to fit the kinetic data. The mathematical equations of these respective models are shown in Eqs. (6), (7), and (8) [34,35].

$$q_t = q_e \cdot [1 - \exp(-k_1 \cdot t)] \quad (6)$$

$$q_t = \frac{q_e^2 k_2 t}{[k_2 (q_e) \cdot t + 1]} \quad (7)$$

$$q_t = q_e \cdot \left\{ 1 - \exp[-(k_{\text{AV}} \cdot t)] \right\}^{\text{nAV}} \quad (8)$$

2.7. Equilibrium of adsorption

The Langmuir, Freundlich, and Liu isotherm models were applied to fit the experimental equilibrium data. The mathematical expression for these models is presented in Eqs. (9)–(11), respectively [34,35].

$$q_e = \frac{Q_{\text{max}} \cdot K_L \cdot C_e}{1 + K_L \cdot C_e} \quad (9)$$

$$q_e = K_F \cdot C_e^{1/n_F} \quad (10)$$

$$q_e = \frac{Q_{\max} \cdot (K_g \cdot C_e)^{n_L}}{1 + (K_g \cdot C_e)^{n_L}} \quad (11)$$

2.8. Synthetic effluents

Two synthetic industrial effluent mixtures were prepared. The effluent consisted of 11 different phenols, humic acid, and inorganics usually present in industrial effluents. The composition of the effluents (A and B) is presented in Table 1. The purpose of using synthetic effluents is to evaluate the sorption capacities of the ASAC for removal of mixed phenolic compounds in the presence of high concentrations of organic matter and salts.

3. Results and discussion

3.1. Characterization of activated carbons

The chemical modification of the AS with $ZnCl_2$ and further pyrolysis assisted by microwave generated ASAC with great structural properties and adsorption capacity when compared with the raw biomass. Among the main

Table 1
Chemical composition of simulated industrial effluents

Phenols	Concentration (mg L ⁻¹)	
	Effluent A	Effluent B
Resorcinol (RES)	50.00	100.0
3-Amino phenol (AMP)	50.00	100.0
Phenol	5.00	10.0
2-Cresol	5.00	10.0
3-Cresol	5.00	10.0
2-Chlorophenol	5.00	10.0
Bisphenol A	5.00	10.0
2-Nitrophenol	5.00	10.0
4-Nitrophenol	5.00	10.0
2-Naphtol	5.00	10.0
Hydroquinone	5.00	10.0
Organic matter		
Humic acid	10.0	20.0
Inorganic components		
Sodium sulfate	20.0	40.0
Sodium carbonate	20.0	40.0
Sodium chloride	20.0	40.0
Potassium nitrate	20.0	40.0
Potassium phosphate	20.0	40.0
pH ^a	7.0	7.0

^apH was adjusted with 1.0 mol L⁻¹ HCl and/or NaOH.

characteristics of the adsorbent, the surface area, and volume of pores play an influential role during adsorption processes. Textural (surface area, porosity, etc.) characterization of the AS and ASAC was performed by N₂ adsorption-desorption isotherms at -196°C and their results are shown in Table 2.

Table 2 presents the surface area, external surface area, micropore area, total pore volume, micropore volume and mesopore volume of the precursor (AS), and ASAC. The porosity characterization displayed that ASAC is composed mainly of mesopores (pores whose diameter are within 2–50 nm) [36]. The total surface area (S_{BET}) of ASAC was 1,433 m² g⁻¹, the surface area due to micropores (S_{micro}) was 279.1 m² g⁻¹, and the external surface was 1,153 m² g⁻¹. It can be seen that only 19.48% of the area of the ASAC is due to the micropores. The total pore volume (V_{tot}) was 0.4447 cm³ g⁻¹, the volume of micropore (V_{mic}) was 0.1189 cm³ g⁻¹, and the volume of mesopores (V_{mes}) was 0.3258 cm³ g⁻¹. The ratio V_{mic}/V_{tot} is 26.74% and the V_{mes}/V_{tot} is 73.26%. It may be observed from these results that the obtained ASAC is predominantly mesoporous with a 26% contribution of micropores [36]. The raw material (AS) presented an S_{BET} value of only 2.776 m² g⁻¹, and it was not possible to measure the area of micropores and volume of micropores and mesopores.

The process of production of activated carbon by chemical activation consists in impregnation of the biomass with $ZnCl_2$. This is followed by a pyrolysis that could occur in a conventional muffle furnace [24,25] or in a microwave oven [22,23] forming a pyrolyzed material containing inorganics [20,23,26,35]. The chemical activation process is conducted using 6.0 mol L⁻¹ HCl [35]. This process increases the porosity of the activated carbon [23]. The role of $ZnCl_2$ in the carbonization of the biomass may be a complexation of this metal with the biomass, followed by a dehydration of the biomass at high temperatures [23,37]. $ZnCl_2$ can melt at >300°C and diffuse to occupy the cavities of the pyrolyzed material. After the pyrolysis, refluxing with 6.0 mol L⁻¹ HCl, would remove the zinc compounds from the cavities of the activated carbon, producing an activated carbon with high porosity and surface area [23,35,37].

It may be noted that the S_{BET} value obtained in this study was higher than other activated carbons reported in the literature reporting different carbon sources as precursor. Dos Reis et al. [19] pyrolyzed sewage sludge, chemically activated it with $ZnCl_2$ and generated an activated carbon with a surface area of 192 m² g⁻¹. Puchana-Rosero et al. [20] produced activated

Table 2
Textural properties of AS and ASAC

Sample	ASAC	AS
S_{BET} (m ² g ⁻¹)	1,433	2.776
S_{micro} (m ² g ⁻¹)	279.1	–
S_{ext} (m ² g ⁻¹)	1,153	–
S_{mic}/S_{BET} (%)	19.48	–
V_{tot} (cm ³ g ⁻¹)	0.4447	0.0069
V_{mic} (cm ³ g ⁻¹)	0.1189	–
V_{mes} (cm ³ g ⁻¹)	0.3258	–
D_p (nm)	2.105	9.918

carbon by microwave pyrolysis of tannery sludge and the S_{BET} of the same was $491 \text{ m}^2 \text{ g}^{-1}$. Saucier et al. [26] produced activated carbon from cocoa shell by microwave-assisted pyrolysis and obtained a material with S_{BET} of $619 \text{ m}^2 \text{ g}^{-1}$. Ribas et al. [35] synthesized biochar from cocoa shell using a conventional furnace and obtained S_{BET} of $522 \text{ m}^2 \text{ g}^{-1}$. The S_{BET} values obtained may depend on the characteristics of the organic precursors, activation method, and the heating procedure. In addition, when chemical activation is used, ZnCl_2 is the most efficient activating agent compared with other metals such as FeCl_3 [26,35], CuCl_2 , CoCl_2 , and NiCl_2 [23]. In order to eliminate the inorganic salts/oxides formed during pyrolysis, the contents were leached out using $6.0 \text{ mol L}^{-1} \text{ HCl}$ [20,22,23,26,35]. Several authors have reported washing with $1.0 \text{ mol L}^{-1} \text{ HCl}$, leading to formation of an activated carbon with lower surface area, and the carbons may release toxic inorganics when in contact with aqueous solutions. On the other hand, the ASAC synthesized in this work was treated with $6.0 \text{ mol L}^{-1} \text{ HCl}$ for leaching inorganics. This was later followed by the treatment with 0.010 M EDTA solution (pH 10.0). The synthesized activated carbon did not release high quantities of Zn into the aqueous solution. The total concentration of Zn leached out from 30.0 mg of ASAC in 20.0 mL of deionized water during 24 h of contact was $0.0240 \pm 0.0006 \text{ mg L}^{-1}$. Considering the permissible limit for Zn that could be available in drinking water is 5.0 mg L^{-1} [38], the concentration of Zn released from the activated carbon was meagre (208 times lower than the permissible limit) [38].

The surface morphology of the materials before (AS) and after pyrolysis (ASAC) was characterized using scanning electron microscopy (SEM). The SEM images of the AS and the ASAC are presented in Fig. 1. The surface of AS is fibrous and smooth (Fig. 1(A)). However, ASAC sample showed a

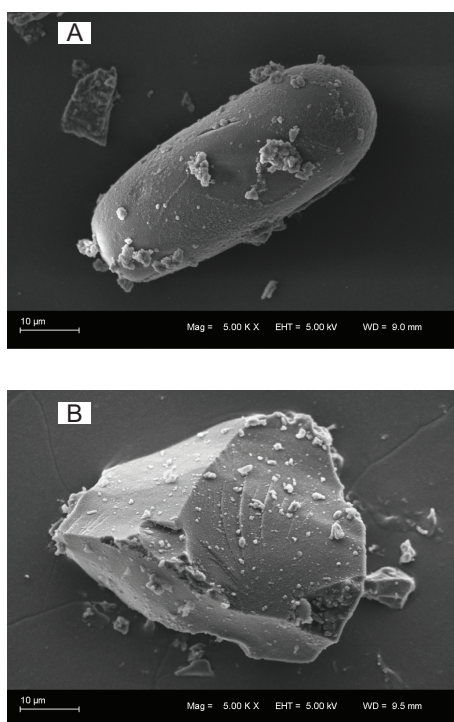


Fig. 1. SEM images of AS and ASAC.

brick of carbon with irregular dimension containing some fissures which may be from the mortar (Fig. 1(B)). SEM technique does not clearly display the pores on the surface of the material because the scale of the figure is micrometers (μm) while, the scale of the pores are in nanometers. Therefore, the N_2 adsorption–desorption curves are a better analytical technique to evaluate the porosity of the adsorbent.

FTIR analysis helps in the identification of the surface functional groups which may contribute toward enhanced adsorption of the pollutant onto the adsorbent [17,22–24]. AS might contain lignin, hemicellulose, cellulose, and tannin as the major components [39]. Thus, a vast numbers of functional groups such as amines, phenolic, carboxyl, and alcohols may exist on the surface and may be involved during the adsorption process [26,39]. The results of FTIR for AS and ASAC are presented in Fig. 2. The AS samples showed the following bands: a band at $3,268 \text{ cm}^{-1}$ is due to the OH stretching vibrations from the intermolecular hydrogen bonding [39]; a band at $2,919 \text{ cm}^{-1}$ is due to the asymmetric C–H stretching, $1,617 \text{ cm}^{-1}$ is due to the asymmetric stretching in (C=O) carboxylates [39], $1,521$ and $1,439 \text{ cm}^{-1}$ may be assigned to the sp^2 hybridized C=C stretching band of the aromatic ring [39]. The band at $1,144$ and $1,003 \text{ cm}^{-1}$ could be assigned to C–O stretching of alcohols or phenols [39], and the band at 762 cm^{-1} could be assigned to C–H out of plane bending in the aromatic rings [39].

FTIR analysis of ASAC showed a broad band at $3,441 \text{ cm}^{-1}$. This band is due to O–H stretching [39]. The bands at $2,921$ and $2,849 \text{ cm}^{-1}$ are due to the asymmetric and symmetric C–H stretching [39]. The band at $1,638 \text{ cm}^{-1}$ is due to the asymmetric stretching in (C=O) carboxylates [39]. The bands at $1,540$ and $1,460 \text{ cm}^{-1}$ could be due to sp^2 hybridized C=C stretching band of the aromatic rings [39], $1,161$ and $1,035 \text{ cm}^{-1}$ may be assigned to C–O stretching in alcohols or phenols [39], and 877 cm^{-1} could be due to C–H out of plane bending mode of the aromatic rings [39].

It could be inferred from the FTIR analysis that the microwave-heating process increased the intermolecular hydrogen bonding otherwise did not bring about much change in the surface groups on ASAC. The major functional groups found in the carbon adsorbent includes: (i) O–H likely from alcohols, phenols, (ii) aromatic rings, (iii)

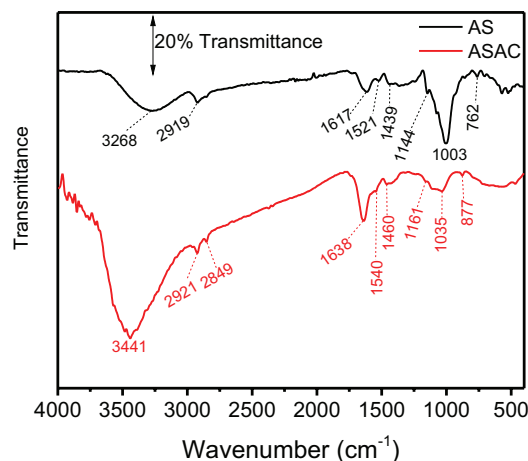


Fig. 2. FTIR spectra of ASAC.

C=O likely from carboxylic acids, esters, and (iv) CH from aromatic and aliphatic compounds may be responsible for the adsorption process.

3.2. Study of adsorbent dosage and initial pH

Preliminary adsorption experiments were carried out with 300 mg L⁻¹ of RES and AMP in order to study higher dosage (0.25–10.0 g L⁻¹) of the ASAC adsorbent. The other conditions such as initial pH was maintained at 6.0 and temperature at 25°C (Supplementary Fig. 3(A)). It was observed for adsorbent dosages ≥ 1.50 g L⁻¹ the percentage of removal of AMP and RES onto ASAC became practically constant. Therefore, this adsorbent dose (1.50 g L⁻¹) was fixed for further experiments (30.0 mg of the adsorbent for 20.0 mL of adsorbate solution). This adsorbent dose is similar to the results reported in our previous studies [20,22,23].

During optimization of pH, the concentration of RES and AMP was kept at 300 mg L⁻¹, adsorbent dosage was 1.5 g L⁻¹, temperature was 25°C, and the pH was varied between 2.0 and 10.0 (Supplementary Fig. 3(B)). It may be seen from Fig. 3(B) that between pH 4 and 9, removal of AMP and RES was practically constant. Hence, it may be concluded that for effluent treatment, it is best to keep the pH close to neutral. Initial pH was maintained at 7.0 in all further experiments.

3.3. Adsorption kinetics

The successful adsorption process depends on proper understanding of the kinetic parameters. Knowledge of the

adsorption kinetics helps to design a process with high efficiency. Kinetic analysis gives us an insight about the interaction/contact between the adsorbate and adsorbent and its significance in the process to attain equilibrium [20,22,39]. After equilibrium is attained, the system reaches a stationary state [20,22,39]. Once stationary state is reached, for practical application, the adsorption may be stopped.

In order to study the kinetics of adsorption of RES and AMP on ASAC, pseudo-first order, pseudo-second order and Avrami fractional order models were applied. The graphical representations of the kinetic models are presented in Fig. 3 and Table 3, respectively.

In order to explain the suitability of the models, their adjusted determination coefficients (R^2_{adj}) and SD of residues were considered. Higher R^2_{adj} and lower SD values mean smaller difference between theoretical and experimental q_t values [19–22,24,26].

On the basis of discussions given above, fractional model has presented the highest R^2_{adj} (varying from 0.9980 to 0.9999) and lowest SD values (varying from 0.6782 to 2.769) for RES and AMP (Table 3) at both initial concentrations, which means that q_t predicted by fractional order model is closer to the values of q_t measured experimentally.

Fractional order model presents a complex or multipathway variations in adsorption mechanism [20,22,40]. The results suggest that the adsorption of RES and AMP onto ASAC, follows multiple kinetic orders instead of an integer-kinetic order [20,22,34,40]. Occurrence of multiple kinetic order of the adsorption is further confirmed by the n_{AV} exponent factor [20,22,34,40].

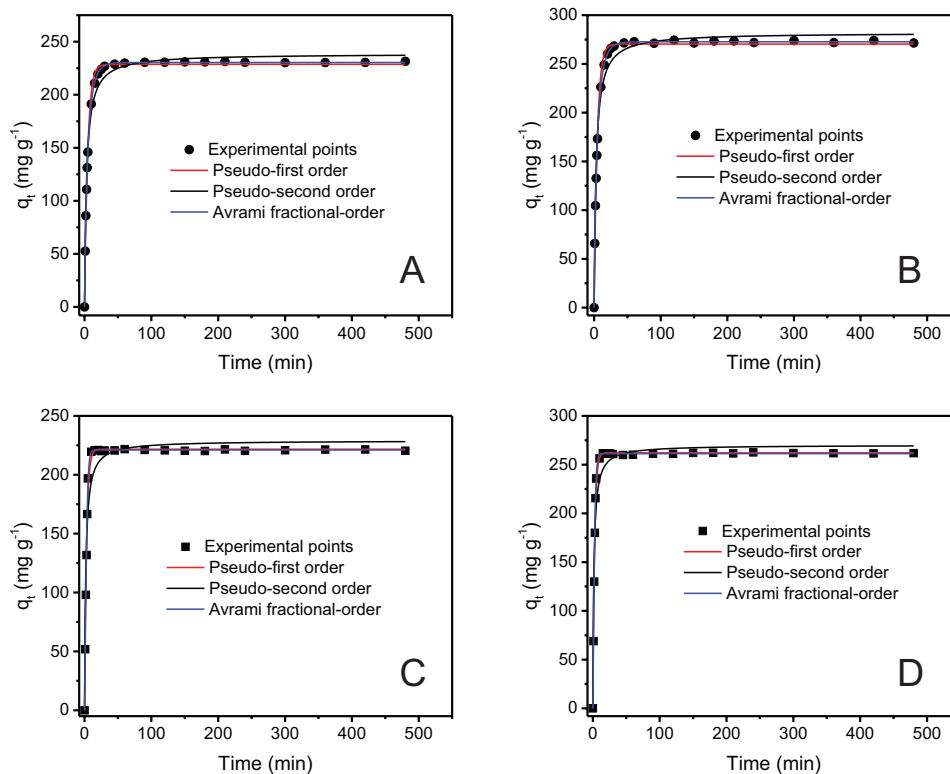


Fig. 3. Adsorption kinetics of AMP at 400 mg L⁻¹ (A) and 900 mg L⁻¹ (B), and RES at 400 mg L⁻¹ (C) and 900 mg L⁻¹ (D) onto ASAC. Conditions: temperature – 25°C, adsorbent mass – 30.0 mg, and initial pH of adsorbate – 7.0.

Table 3
Kinetic parameters for adsorption of RES and AMP onto ASAC

	RES		AMP	
	400.0 mg L ⁻¹	900.0 mg L ⁻¹	400.0 mg L ⁻¹	900.0 mg L ⁻¹
Pseudo-first order				
k_f (min ⁻¹)	0.3287	0.3826	0.2110	0.2149
q_e (mg g ⁻¹)	221.7	262.1	228.7	270.4
$t_{1/2}$	2.109	1.812	3.285	3.226
$t_{0.95}$	9.114	7.831	14.20	13.94
R^2 adjusted	0.9921	0.9943	0.9957	0.9945
SD (mg g ⁻¹)	5.492	5.274	4.443	5.916
Pseudo-second order				
k_s (g mg ⁻¹ min ⁻¹)	0.002367	0.002406	0.001373	0.01191
q_e (mg g ⁻¹)	229.0	270.1	238.7	282.0
$t_{1/2}$	1.845	1.539	3.052	2.977
$t_{0.95}$	35.05	29.24	57.98	56.57
R^2 adjusted	0.9513	0.9558	0.9890	0.9894
SD (mg g ⁻¹)	13.62	14.73	7.098	8.190
Avrami fractional order				
k_{AV} (min ⁻¹)	0.3310	0.3810	0.1999	0.2027
q_e (mg g ⁻¹)	221.0	261.3	230.4	272.7
n_{AV}	1.296	1.270	0.8232	0.8043
$t_{1/2}$	2.277	1.967	3.206	3.128
$t_{0.95}$	7.046	6.226	18.97	19.30
R^2 adjusted	0.9980	0.9996	0.9999	0.9999
SD (mg g ⁻¹)	2.769	1.452	0.6782	0.8730

Conditions: Initial pH of adsorbate – 7.0, adsorbent mass – 30 mg.

Considering that the kinetic models present different rate constants with different units, it is difficult to compare the rate constants of these models. Considering $t_{1/2}$ and $t_{0.95}$ are the time necessary to attain 50% and 95% of the saturation, respectively [22,26], the kinetic equation constants were calculated based on the nonlinear interpolation of their respective kinetic curves of Fig. 3 (Table 3). Considering the above discussion, Avrami fractional model is the best fit for the experimental data. In the case of RES, the $t_{1/2}$ values ranged from 1.967 to 2.277 min, and $t_{0.95}$ ranged from 6.226 to 7.046 min. While, in the case of AMP, the $t_{1/2}$ values ranged from 3.128 to 3.206 min and $t_{0.95}$ ranged from 18.97 to 19.30 min. Based on these values of $t_{1/2}$ and $t_{0.95}$ it is possible to infer that the kinetics of adsorption of RES is more rapid than AMP. The increase of initial adsorbate concentration could increase the time required to reach equilibrium [34]. Based on these results, the contact time between the adsorbent and adsorbate for the experiments was fixed at 30 min for RES and 60 min for AMP.

3.4. Adsorption isotherms

The adsorption isotherms play a significant role in understanding how the adsorbates interact with adsorbents and it helps with the enhanced use of the adsorbent. An adsorption isotherm defines the interaction between the quantity of adsorbate adsorbed and the concentration of adsorbate that was left unadsorbed in solution, at a fixed temperature. Nonlinear forms of Langmuir, Freundlich, and Liu isotherm models were used to study the adsorption data of RES and AMP [34], and the results are presented in Fig. 4 and Table 4.

As done in the previous kinetic studies [20,22], the most suited equilibrium model was determined using the adjusted determination coefficient (R^2_{adj}) and SD of residues.

On the basis of R^2_{adj} and SD values, the best fitting model for both RES and AMP onto ASAC was the Liu isotherm model. The model presented R^2_{adj} closer to 1.00 and the lowest SD values, which interprets that the q predicted by the Liu isotherm model is closer to the experimentally

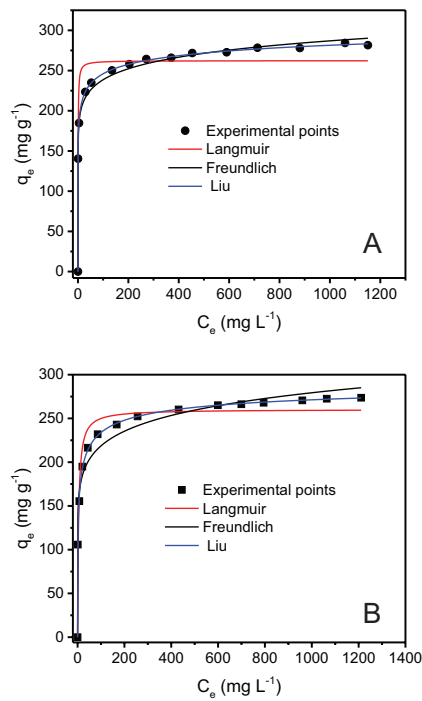


Fig. 4. Adsorption isotherms of AMP (A) and RES (B) onto ASAC at 25°C. Conditions: adsorbent mass – 30.0 mg, initial pH of adsorbate – 7.0, time of contact between the adsorbent and adsorbate – 30 min for RES and 60 min for AMP.

measured q . At all studied range temperatures, both RES and AMP followed Liu isotherm model [20,22,34].

The maximum adsorption capacity calculated by using the Liu model was observed to be 299.7, 317.4, 332.1, 349.0, 366.8, and 406.2 mg g^{-1} at 25°C, 30°C, 35°C, 40°C, 45°C, and 50°C for RES, respectively. The maximum adsorption capacity values observed for AMP were 352.4, 372.1, 390.4, 410.6, 432.0, and 454.5 mg g^{-1} at 25°C, 30°C, 35°C, 40°C, 45°C, and 50°C, respectively. These values are closest to experimental data because presented highest R^2_{adj} and lowest SD values (Table 4).

3.5. Comparative evaluation of adsorption of phenolic compounds on activated carbons and other adsorbents

The maximum adsorption efficiency of ASAC was compared with various others adsorbents reported in literature [41–50] and presented in Table 5. It is obvious from Table 5 that the ASAC exhibited higher adsorption capacities for both adsorbates RES and AMP. Among the 12 different adsorbents presented in the table, ASAC exhibited a Q_{max} value $>400 \text{ mg g}^{-1}$ which is higher than 11 other materials presented in the table. Although the Q_{max} values of the carbons presented in the table were derived at different experimental conditions, the values were obtained in their best-optimized conditions and are being compared with the best-optimized conditions of this work. These results are significant from a scientific point of view, because the adsorbents proposed in this present study show very good performance when matched with

Table 4
Langmuir, Freundlich, and Liu isotherm parameters for the adsorption of RES and AMP onto ASAC

	Resorcinol						3-Aminophenol					
	25°C	30°C	35°C	40°C	45°C	50°C	25°C	30°C	35°C	40°C	45°C	50°C
Langmuir												
Q_{max} (mg g^{-1})	260.3	278.4	280.6	293.0	312.2	315.2	262.3	271.5	289.0	338.8	311.8	314.2
K_L (L mg^{-1})	0.2403	0.2530	0.1296	0.1630	0.1408	0.2077	1.687	0.8502	0.6203	0.2930	0.6140	0.2173
R^2_{adj}	0.9417	0.9589	0.9728	0.9606	0.9595	0.9419	0.9179	0.9210	0.9576	0.9203	0.9243	0.9799
SD (mg g^{-1})	18.73	17.58	12.39	16.90	18.71	22.77	21.72	21.65	16.23	28.82	24.17	11.54
Freudlich												
K_F (mg g^{-1} (mg L^{-1}) $^{-1/n_F}$)	133.9	130.4	151.5	138.3	139.1	147.1	164.9	172.6	181.4	177.8	190.1	207.1
n_F	9.394	7.980	10.15	8.121	7.507	7.911	12.47	13.17	12.57	9.136	11.51	14.62
R^2_{adj}	0.9710	0.9649	0.9907	0.9824	0.9729	0.9872	0.9922	0.9954	0.9966	0.9759	0.9949	0.9993
SD (mg g^{-1})	13.20	16.24	7.235	11.29	15.30	10.68	6.686	5.230	4.614	15.84	6.260	2.128
Liu												
Q_{max} (mg g^{-1})	299.7	317.4	332.1	349.0	366.8	406.2	352.4	372.1	390.4	410.6	432.0	454.5
K_g (L mg^{-1})	0.1922	0.1579	0.1308	0.1088	0.09326	0.07958	0.3576	0.2903	0.2593	0.2186	0.1842	0.1549
n_L	0.4289	0.4910	0.4052	0.4349	0.4853	0.3662	0.2344	0.2182	0.2371	0.3652	0.2466	0.1918
R^2_{adj}	0.9990	0.9998	0.9997	0.9998	0.9999	0.9997	0.9997	0.9999	0.9999	0.9999	0.9999	0.9999
SD (mg g^{-1})	2.428	1.152	1.234	1.231	1.137	1.585	1.389	0.3177	0.3353	0.4664	0.03385	0.03534

Conditions: Adsorbent mass – 30.0 mg, initial pH of adsorbate – 7.0, time of contact – 30 min for RES and 60 min for AMP.

adsorbents already reported in the literature [41–50]. This shows that the AS raw material can generate an efficient activated carbon for removal of phenolic compounds from aqueous solutions.

3.6. Effect of temperature and thermodynamic parameters

The effect of temperature is another essential physico-chemical variable that can influence adsorption. Variation in temperature of the reaction would directly impact change in

the adsorption efficiency and the adsorption capacity of the adsorbent [34,35,39].

The effect of temperature on the removal of the phenolic compounds by ASAC was investigated by varying the temperature from 25°C to 50°C (Table 6). Adsorption of both the phenolic compounds seemed to be significantly affected by temperature and the same influenced the Q_{\max} values (Table 4). During RES adsorption, the Q_{\max} at 25°C was 299.7 mg g⁻¹. It increased to 406.2 mg g⁻¹ at 50°C, an enhancement of 35.53% was observed on the maximum adsorption

Table 5
Maximum sorption capacities of different adsorbents used for removal of various phenolic compounds

Adsorbent	Phenolic adsorbate	Q_{\max} (mg g ⁻¹)	References
Mesoporous SBA-15	Resorcinol	128	[41]
Mesoporous carbon	Resorcinol	37	[42]
Mesoporous carbon	Resorcinol	39.2	[43]
Activated carbon coal	3-Aminophenol	110	[44]
Mesoporous carbons	Resorcinol	40.6	[45]
Activated carbon from waste rubber	<i>p</i> -Cresol	250	[46]
Eggshell activated carbons	Phenol	192	[47]
Activated carbon	2-Chlorophenol	549.5	[48]
Aminated activated carbons	Phenol	227.27	[49]
Granular activated carbon	Catechol	100	[49]
Granular activated carbon	Resorcinol	113	[50]
ASAC	Resorcinol	406.2	This work
ASAC	3-Aminophenol	454.5	This work

Table 6
Thermodynamic parameters of the adsorption of resorcinol (RES) and 3-aminophenol (AMP) onto ASAC

	Temperature (K)					
	298	303	308	313	318	323
Resorcinol						
K_g (L mol ⁻¹)	2,116	1,738	1,440	1,198	1,027	876.2
ΔG° (kJ mol ⁻¹)	-24.68	-24.60	-24.52	-24.44	-24.42	-24.38
ΔH° (kJ mol ⁻¹)	-28.25	-	-	-	-	-
ΔS° (J K ⁻¹ mol ⁻¹)	-12.06	-	-	-	-	-
R^2_{adj}	0.9991	-	-	-	-	-
3-Aminophenol						
K_g (L mol ⁻¹)	3,902	3,168	2,830	2,386	2,010	1,690
ΔG° (kJ mol ⁻¹)	-26.19	-26.11	-26.25	-26.23	-26.20	-26.14
ΔH° (kJ mol ⁻¹)	-26.14	-	-	-	-	-
ΔS° (J K ⁻¹ mol ⁻¹)	0.1346	-	-	-	-	-
R^2_{adj}	0.9942	-	-	-	-	-

capacity (Table 4). The same trend was observed for the AMP. At 25°C, the Q_{\max} for AMP was 352.4 and when the temperature was raised to 50°C the maximum adsorption capacity achieved was 454.5 mg g⁻¹. An enhancement of 28.97% on the maximum adsorption capacity was observed. Although there is an increase in the Q_{\max} values of both adsorbates with the increase of temperature, there is no relationship of this parameter with the thermodynamics of adsorption, as reported in an earlier publication [34]. On the other hand, the equilibrium constant of the Liu model decreased uniformly with the increase in temperature, demonstrating that the adsorption in AMP and RES were exothermic. In order to validate the above statement, the thermodynamic parameters for RES and AMP adsorption are presented in Table 6.

Change in enthalpy and entropy (ΔH° and ΔS°) can be calculated from the slope and the intercept of the plot of $\ln K_c$ vs. $1/T$ [34,35,39]. The R^2_{adj} values of the plots are 0.9942 and 0.9991 for AMP and RES, respectively.

The interactions of adsorbent with adsorbate can be chemical or physical. This may be explained using the magnitude of enthalpy. The enthalpy value for physical adsorption is <40 kJ mol⁻¹ [51]. The enthalpy values of adsorption of RES and AMP onto the activated carbon is compatible with the physical adsorption [51]. ΔH° has negative values, which signify that the interactions of the activated carbon with RES and AMP are exothermic. Since ΔG° values are negative the adsorption of RES and AMP onto ASAC is spontaneous, and a favorable process.

3.7. Removal of simulated mixed phenolic effluent using ASAC

Two mixtures of synthetic effluents containing various phenolic compounds, humic acid, and some inorganic salts with different compositions were prepared. The efficacy of the ASAC as an adsorbent to treat synthetic effluents was investigated (Table 1).

The UV–Vis spectra of the untreated and treated effluents were observed from 190 to 500 nm (Fig. 5). The percentage removal of the phenolic compounds from the synthetic effluents was calculated using the area under the absorption bands. ASAC displayed great adsorption performance on the removal of both the synthetic effluent mixtures. The removal percentages were 99.33% and 96.94% for effluent A and effluent B, respectively.

Based on the above results obtained from simulated effluent, ASAC may be an efficient adsorbent for the removal of phenolic compounds from simulated wastewaters as well as industrial effluents contaminated with organic compounds [52–55].

4. Conclusion

In this work, ASAC was prepared by microwave-heating process after chemical activation with ZnCl₂ as activating agent. The produced activated carbon exhibited high specific surface area 1,433 m² g⁻¹. The S_{BET} results show that ASAC possessed 19.48% of micropores and 80.52% of external surface. In relation to volume of pores, 26.74% of pore volume corresponded to micropores and 73.26% to mesopores. Therefore, the ASAC synthesized in this research study may be classified as predominantly mesoporous.

The adsorptive capacity of ASAC was evaluated using RES and AMP removal percentages. Avrami fractional

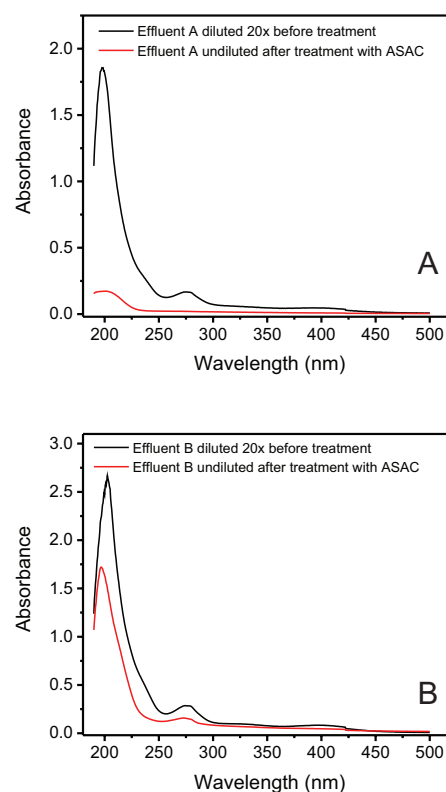


Fig. 5. UV/Vis spectra of simulated effluents A and B before and after treatment with ASAC activated carbon. See Table 1 for the composition of the effluents.

order and Liu isotherm model were found to be best fit to the experimental data. According to Liu isotherm model, the maximum adsorption capacity achieved were 406.2 and 454.5 mg g⁻¹ for RES and AMP at 50°C, respectively. This adsorption capacity values were found to be highest among the ones reported in literature [41–50].

It was seen from the effect of temperature and thermodynamic data, that the adsorption processes of RES and AMP onto ASAC were dependent on temperature. The adsorption process was exothermic and spontaneous.

The avocado-activated carbon displayed excellent removal of simulated phenolic effluents; they effectively removed >96.94% of a mixture containing high concentrations of phenols, organic matter, and salinity. It may be concluded that, ASAC can be effectively used in real wastewater contaminated with phenolic compounds.

Acknowledgments

The authors are grateful to The Coordination of Improvement of Higher Education Personnel (CAPES, Brazil), to The Academy of Sciences for Developing World (TAS, Italy), and to The National Council for Scientific and Technological Development (CNPq, Brazil), to Clean Water Mission Project (ESC – 00306), CSIR-NEERI, India for sponsorship and fellowships. We are also grateful to Centre of Electron Microscopy (CME-UFRGS) for the use of the SEM microscope. We are grateful to Chemaxon for giving us an academic research license for the MarvinSketch software,

Version 16.6.6.0, (<http://www.chemaxon.com>), 2016 used for phenols physical–chemical properties.

Symbols and acronyms

AS	—	Avocado seed
ASAC	—	Avocado seed activated carbon
RES	—	Resorcinol
AMP	—	3-Aminophenol
FTIR	—	Fourier transform infrared spectroscopy
SEM	—	Scanning electron microscopy
BET	—	Brunauer, Emmett and Teller method for determination of surface area
BET method	—	Total Surface area determined by BET method, $\text{m}^2 \text{g}^{-1}$
S_{BET}	—	Total Surface area determined by BET method, $\text{m}^2 \text{g}^{-1}$
S_{micro}	—	Surface area of micropores obtained by t plot, $\text{m}^2 \text{g}^{-1}$
S_{external}	—	External surface area, $\text{m}^2 \text{g}^{-1}$
S_{BET}	—	$S_{\text{micro}} + S_{\text{external}}$
V_{tot}	—	Total volume of pores, $\text{cm}^3 \text{g}^{-1}$
V_{micro}	—	Volume of micropores, $\text{cm}^3 \text{g}^{-1}$
V_{meso}	—	Volume of mesopores, $\text{cm}^3 \text{g}^{-1}$
V_{tot}	—	$V_{\text{micro}} + V_{\text{meso}}$
R^2	—	Coefficient of determination
R^2_{adj}	—	Adjusted coefficient of determination
SD	—	Standard deviation of the residues
q	—	Sorption capacity of phenolic compounds adsorbed, mg g^{-1}
C_0	—	Initial adsorbate concentration, mg L^{-1}
C_f	—	Adsorbate concentrations in equilibrium, mg L^{-1}
m	—	Weight of ASAC, g
V	—	Volume of the adsorbate in solution, L
$q_{i, \text{exp}}$	—	Distinct experimental q value
\bar{q}_{exp}	—	Mean experimental q values
$q_{i, \text{model}}$	—	Distinct theoretical q value predicted by the model
n	—	Number of experiments
p	—	Number of variables in the model
q_e	—	Amount of adsorbate adsorbed at the equilibrium, mg g^{-1}
C_e	—	Supernatant adsorbate concentration at the equilibrium, mg L^{-1}
K_L	—	Langmuir equilibrium constant, L mg^{-1}
Q_{max}	—	Maximum adsorption capacity of the adsorbent, mg g^{-1}
K_F	—	Freundlich equilibrium constant, $\text{mg g}^{-1} (\text{mg L}^{-1})^{-1/n}$
n_F	—	Freundlich exponent, dimensionless
K_s	—	Liu equilibrium constant, L mg^{-1}
n_L	—	Dimensionless exponent of the Liu equation
q_t	—	Amount of adsorbate adsorbed at time t , mg g^{-1}
q_e	—	Equilibrium adsorption capacity, mg g^{-1}
k_f	—	Pseudo-first-order rate constant, min^{-1}
t	—	Contact time, min
k_s	—	Pseudo-second-order rate constant, $\text{g mg}^{-1} \text{min}^{-1}$
k_{AV}	—	Avrami kinetic constant, min^{-1}

n_{AV}	—	Fractional adsorption order, which is related to the adsorption mechanism
$t_{1/2}$	—	Time necessary to attain 50% of the saturation
$t_{0.95}$	—	Time necessary to attain 95% of the saturation

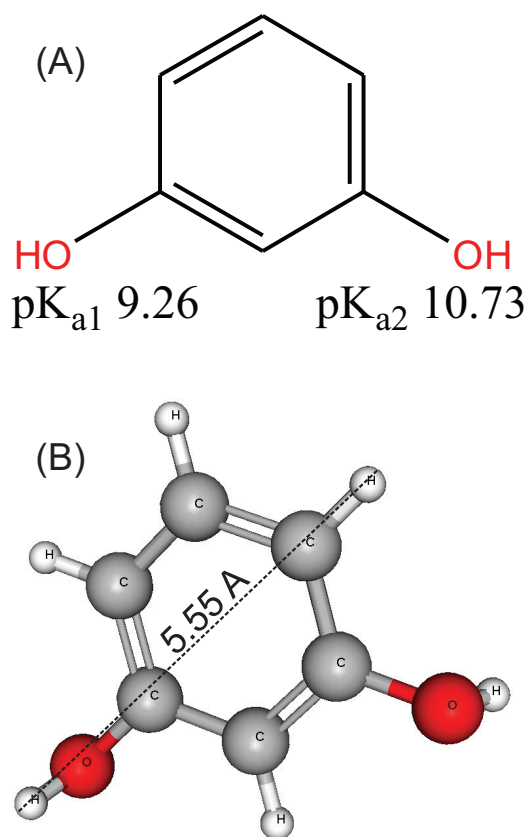
References

- [1] S. Kottuparambil, Y.J. Kim, H. Choi, M.S. Kim, A. Park, J. Park, W. Shin, T. Han, A rapid phenol toxicity test based on photosynthesis and movement of the freshwater flagellate, *Euglena agilis* Carter, *Aquat. Toxicol.*, 155 (2014) 9–14.
- [2] M.D. Erturk, M.T. Saçan, Assessment and modeling of the novel toxicity data set of phenols to *Chlorella vulgaris*, *Ecotoxicol. Environ. Saf.*, 90 (2013) 61–68.
- [3] Y. Liu, M. Meng, J. Yao, Z. Da, Y. Feng, Y. Yan, C. Li, Selective separation of phenol from salicylic acid effluent over molecularly imprinted polystyrene nanospheres composite alumina membranes, *Chem. Eng. J.*, 286 (2016) 622–631.
- [4] E.B. Estrada-Arriaga, J.A. Zepeda-Aviles, L. García-Sánchez, Post-treatment of real oil refinery effluent with high concentrations of phenols using photo-ferrioxalate and Fenton's reactions with membrane process step, *Chem. Eng. J.*, 285 (2016) 508–516.
- [5] N. Wang, T. Zheng, G. Zhang, P. Wang, A review on Fenton-like processes for organic wastewater treatment, *J. Environ. Chem. Eng.*, 4 (2016) 762–787.
- [6] N. Jarrah, N.D. Múazu, Simultaneous electro-oxidation of phenol, CN^- , S^{2-} and NH_4^+ in synthetic wastewater using boron doped diamond anode, *J. Environ. Chem. Eng.*, 4 (2016) 2656–2664.
- [7] R. Boonchai, G. Seo, Microalgae membrane photobioreactor for further removal of nitrogen and phosphorus from secondary sewage effluent, *Korean J. Chem. Eng.*, 32 (2015) 2047–2052.
- [8] A. Hussain, S. K. Dubey, V. Kumar, Kinetic study for aerobic treatment of phenolic wastewater, *Water Resour. Ind.*, 11 (2015) 81–90.
- [9] R. Muppalla, S.K. Jewrajka, A.V.R. Reddy, Fouling resistant nanofiltration membranes for the separation of oil–water emulsion and micropollutants from water, *Sep. Purif. Technol.*, 143 (2015) 125–134.
- [10] J.J. Rueda-Márquez, M.G. Pintado-Herrera, M.L. Martín-Díaz, A. Acevedo-Merino, M.A. Manzano, Combined AOPs for potential wastewater reuse or safe discharge based on multi-barrier treatment (microfiltration- H_2O_2 /UV-catalytic wet peroxide oxidation), *Chem. Eng. J.*, 270 (2015) 80–90.
- [11] L. Ma, J. Zhua, Y. Xi, R. Zhu, H. He, X. Liang, G.A. Ayoko, Adsorption of phenol, phosphate and Cd(II) by inorganic-organic montmorillonites: a comparative study of single and multiple solute, *Colloids Surf., A*, 497 (2016) 63–71.
- [12] Z. Luo, M. Gao, S. Yang, Q. Yang, Adsorption of phenols on reduced-charge montmorillonites modified by bispyridinium dibromides: mechanism, kinetics and thermodynamics studies, *Colloids Surf., A*, 482 (2015) 222–230.
- [13] V. Makrigianni, A. Giannakas, Y. Deligiannakis, I. Konstantinou, Adsorption of phenol and methylene blue from aqueous solutions by pyrolytic tire char: equilibrium and kinetic studies, *J. Environ. Chem. Eng.*, 3 (2015) 574–582.
- [14] L.D.T. Prola, E. Acayanka, E.C. Lima, C.S. Umpierrez, J.C.P. Vagheti, W.O. Santos, S. Laminsi, P.T. Njifon, Comparison of *Jatropha curcas* shells in natural form and treated by non-thermal plasma as biosorbents for removal of Reactive Red 120 textile dye from aqueous solution, *Ind. Crops Prod.*, 46 (2013) 328–340.
- [15] M. Shirmardi, A.H. Mahvi, B. Hashemzadeh, A. Naeimabadi, G. Hassani, M.V. Niri, The adsorption of malachite green (MG) as a cationic dye onto functionalized multi walled carbon nanotubes, *Korean J. Chem. Eng.*, 30 (2013) 1603–1608.
- [16] D. Pérez-Quintanilla, A. Sánchez, I. Sierra, Preparation of hybrid organic-inorganic mesoporous silicas applied to mercury

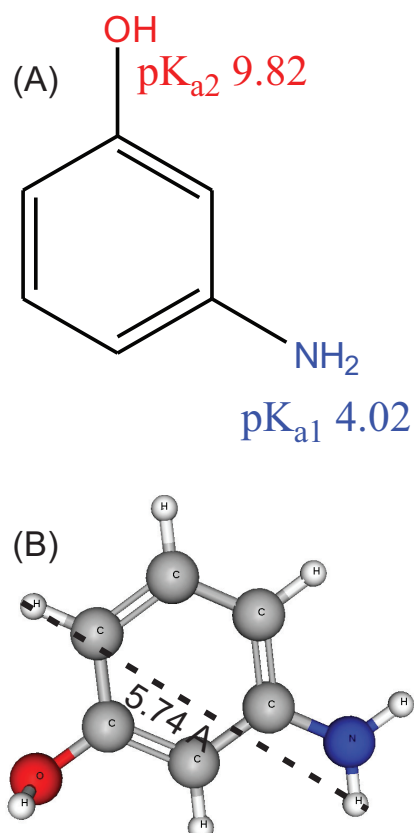
- removal from aqueous media: influence of the synthesis route on adsorption capacity and efficiency, *J. Colloid Interface Sci.*, 472 (2016) 126–134.
- [17] G.S. dos Reis, C.H. Sampaio, E.C. Lima, M. Wilhelm, Preparation of novel adsorbents based on combinations of polysiloxanes and sewage sludge to remove pharmaceuticals from aqueous solutions, *Colloids Surf., A*, 497 (2016) 304–315.
- [18] L. Wanga, C. Han, M.N. Nadagouda, D.D. Dionysiou, An innovative zinc oxide-coated zeolite adsorbent for removal of humic acid, *J. Hazard. Mater.*, 313 (2016) 283–290.
- [19] G.S. dos Reis, M. Wilhelm, T.C.A. Silva, K. Rezwan, C.H. Sampaio, E.C. Lima, S.M.A.G.U. Souza, The use of design of experiments for the evaluation of the production of surface rich activated carbon from sewage sludge via microwave and conventional pyrolysis, *Appl. Therm. Eng.*, 93 (2016) 590–597.
- [20] M.J. Puchana-Rosero, M.A. Adebayo, E.C. Lima, F.M. Machado, P.S. Thue, J.C.P. Vagheti, G.S. Umpierrez, M. Gutierrez, Microwave-assisted activated carbon obtained from the sludge of tannery-treatment effluent plant for removal of leather dyes, *Colloids Surf., A*, 504 (2016) 105–115.
- [21] M.S. Bretanha, M.C. Rochefort, G.L. Dotto, E.C. Lima, S.L.P. Dias, F.A. Pavan, *Punica granatum* husk (PGH), a powdered bio-waste material for the adsorption of methylene blue dye from aqueous solution, *Desal. Wat. Treat.*, 57 (2016) 3194–3204.
- [22] P.S. Thue, M.A. Adebayo, E.C. Lima, J.M. Sieliechi, F.M. Machado, G.L. Dotto, J.C.P. Vagheti, S.L.P. Dias, Preparation, characterization and application of microwave-assisted activated carbons from wood chips for removal of phenol from aqueous solution, *J. Mol. Liq.*, 223 (2016) 1067–1080.
- [23] P.S. Thue, E.C. Lima, J.M. Sieliechi, C. Saucier, S.L.P. Dias, J.C.P. Vagheti, F.S. Rodembusch, F.A. Pavan, Effects of first-row transition metals and impregnation ratios on the physicochemical properties of microwave-assisted activated carbons from wood biomass, *J. Colloid Interface Sci.*, 486 (2017) 163–175.
- [24] T. Calvete, E.C. Lima, N.F. Cardoso, S.L.P. Dias, E.S. Ribeiro, Removal of brilliant green dye from aqueous solutions using home made activated carbons, *Soil Air Water*, 38 (2010) 521–532.
- [25] A. Takdastan, A.H. Mahvi, E.C. Lima, M. Shirmardi, A.A. Babaei, G. Goudarzi, A. Neisi, M.H. Farsani, M. Vosoughi, Preparation, characterization, and application of activated carbon from low-cost material for the adsorption of tetracycline antibiotic from aqueous solutions, *Water Sci. Technol.*, 74 (2016) 2349–2363.
- [26] C. Saucier, M.A. Adebayo, E.C. Lima, R. Cataluna, P.S. Thue, L.D.T. Prola, M.J. Puchana-Rosero, F.M. Machado, F.A. Pavan, G.L. Dotto, Microwave-assisted activated carbon from cocoa shell as adsorbent for removal of sodium diclofenac and nimesulide from aqueous effluents, *J. Hazard. Mater.*, 289 (2015) 18–27.
- [27] Z.Z. Qiang, X.H. Ying, C. Srinivasakannan, P.J. Hui, Z.L. Bo, Utilization of Crofton weed for preparation of activated carbon by microwave induced CO₂ activation, *Chem. Eng. Process.*, 82 (2014) 1–8.
- [28] N. Ferrera-Lorenzo, E. Fuente, I. Suárez-Ruiz, B. Ruiz, KOH activated carbon from conventional and microwave heating system of a macroalgae waste from the Agar–Agar industry, *Fuel Process. Technol.*, 121 (2014) 25–31.
- [29] R.H. Hesas, W.M.A.W. Daud, J.N. Sahu, A.A. Niya, The effects of a microwave heating method on the production of activated carbon from agricultural waste: a review, *J. Anal. Appl. Pyrolysis*, 100 (2013) 1–11.
- [30] F. Barbosa Jr., E.C. Lima, F.J. Krug, Determination of arsenic in sediment and soil slurries by electrothermal atomic absorption spectrometry using W-Rh permanent modifier, *Analyst*, 125 (2000) 2079–2083.
- [31] E.C. Lima, R.V. Barbosa, J.L. Brasil, A.H.D.P. Santos, Evaluation of different permanent modifiers for the determination of arsenic, cadmium and lead in environmental samples by electrothermal atomic absorption spectrometry, *J. Anal. At. Spectrom.*, 17 (2002) 1523–1529.
- [32] E.C. Lima, J.L. Brasil, A.H.D.P. Santos, Evaluation of Rh, Ir, Ru, W–Rh, W–Ir and W–Ru as permanent modifiers for the determination of lead in ashes, coals, sediments, sludges, soils, and freshwaters by electrothermal atomic absorption spectrometry, *Anal. Chim. Acta*, 484 (2003) 233–242.
- [33] E.C. Lima, F.J. Krug, J.A. Nóbrega, A.R.A. Nogueira, Determination of ytterbium in animal faeces by tungsten coil electrothermal atomic absorption spectrometry, *Talanta*, 47 (1998) 613–623.
- [34] E.C. Lima, M.A. Adebayo, F.M. Machado, Kinetic and Equilibrium Models of Adsorption, Chapter 3, C.P. Bergmann, F.M. Machado, Ed., Carbon Nanomaterials as Adsorbents for Environmental and Biological Applications, Springer (Springer International Publishing, Switzerland), 2015, pp. 33–69.
- [35] M.C. Ribas, M.A. Adebayo, L.D.T. Prola, E.C. Lima, R. Cataluña, L.A. Feris, M.J. Puchana-Rosero, F.M. Machado, F.A. Pavan, T. Calvete, Comparison of a homemade cocoa shell activated carbon with commercial activated carbon for the removal of reactive violet 5 dye from aqueous solutions, *Chem. Eng. J.*, 248 (2014) 315–326.
- [36] P.B. Balbuenat, K.E. Gubbins, Theoretical interpretation of adsorption behavior of simple fluids in slit pores, *Langmuir*, 9 (1993) 1801–1814.
- [37] H. Shang, Y. Lu, F. Zhao, C. Chao, B. Zhang, H. Zhang, Preparing high surface area porous carbon from biomass by carbonization in a molten salt medium, *RSC Adv.*, 5 (2015) 75728–75734.
- [38] Drinking Water Contaminants – Standards and Regulations – Secondary Drinking Water Standards: Guidance for Nuisance Chemicals, United States Environmental Protection Agency. Available at: <https://www.epa.gov/dwstandardsregulations/secondary-drinking> (Accessed January 18, 2017).
- [39] A. Bazzo, M.A. Adebayo, S.L.P. Dias, E.C. Lima, J.C.P. Vagheti, E.R. de Oliveira, A.J.B. Leite, F.A. Pavan, Avocado seed powder: characterization and its application for crystal violet dye removal from aqueous solutions, *Desal. Wat. Treat.*, 57 (2016) 15873–15888.
- [40] E.C. Lima, A.R. Cestari, M.A. Adebayo, Comments on the paper: a critical review of the applicability of Avrami fractional kinetic equation in adsorption-based water treatment studies, *Desal. Wat. Treat.*, 57 (2016) 19566–19571.
- [41] Q. Li, H. Yu, J. Song, X. Pan, J. Liu, Y. Wang, L. Tang, Synthesis of SBA-15/polyaniline mesoporous composite for removal of resorcinol from aqueous solution, *Appl. Surf. Sci.*, 290 (2014) 260–266.
- [42] W. Shou, B. Chao, Z.U. Ahmad, D.D. Gang, Ordered mesoporous carbon preparation by the in situ radical polymerization of acrylamide and its application for resorcinol removal, *J. Appl. Polym. Sci.*, 133 (2016). doi: 10.1002/app.43426.
- [43] R. Guo, J. Guo, F. Yu, D.D. Gang, Synthesis and surface functional group modifications of ordered mesoporous carbons for resorcinol removal, *Microporous Mesoporous Mater.*, 175 (2013) 141–146.
- [44] B. Petrova, B. Tsyntsarski, T. Budinova, N. Petrova, L.F. Velasco, C.O. Ania, Activated carbon from coal tar pitch and furfural for the removal of p-nitrophenol and m-aminophenol, *Chem. Eng. J.*, 172 (2011) 102–108.
- [45] H. Ren, W. Shou, C. Ren, D.D. Gang, Preparation and post-treatments of ordered mesoporous carbons (OMC) for resorcinol removal, *Int. J. Environ. Sci. Technol.*, 13 (2016) 1505–1514.
- [46] V.K. Gupta, A. Nayak, S. Agarwal, I. Tyagi, Potential of activated carbon from waste rubber tire for the adsorption of phenolics: effect of pre-treatment conditions, *J. Colloid Interface Sci.*, 417 (2014) 420–430.
- [47] L. Giraldo, J.C. Moreno-Piraján, Study of adsorption of phenol on activated carbons obtained from eggshells, *J. Anal. Appl. Pyrolysis*, 106 (2014) 41–47.
- [48] P. Strachowski, M. Bystrzejewski, Comparative studies of sorption of phenolic compounds onto carbon-encapsulated iron nanoparticles, carbon nanotubes and activated carbon, *J. Mol. Liq.*, 213 (2016) 351–359.
- [49] G. Yang, H. Chen, H. Qin, Y. Feng, Amination of activated carbon for enhancing phenol adsorption: effect of nitrogen-containing functional groups, *Appl. Surf. Sci.*, 293 (2014) 299–305.
- [50] S. Suresh, V.C. Srivastava, I.M. Mishra, Study of catechol and resorcinol adsorption mechanism through granular activated

- carbon: characterization, pH and kinetic study, *Sep. Sci. Technol.*, 46 (2011) 1750–1766.
- [51] C.L. Sun, C.S. Wang, Estimation on the intramolecular hydrogen-bonding energies in proteins and peptides by the analytic potential energy function, *J. Mol. Struct.*, 956 (2010) 38–43.
- [52] M. Shirmardi, N. Alavi, E.C. Lima, A. Takdastan, A.H. Mahvi, A.A. Babaei, Removal of atrazine as an organic micro-pollutant from aqueous solutions: a comparative study, *Process Saf. Environ. Prot.*, 103 (2016) 23–35.
- [53] A.A. Babaei, E.C. Lima, A. Takdastan, N. Alavi, G. Goudarzi, M. Vosoughi, G. Hassani, M. Shirmardi, Removal of tetracycline antibiotic from contaminated water media by multi-walled carbon nanotubes: operational variables, kinetics, and equilibrium studies, *Water Sci. Technol.*, 74 (2016) 1202–1216.
- [54] M. Shirmardi, A.H. Mahvi, A. Mesdaghinia, S. Nasser, R. Nabizadeh, Adsorption of acid red 18 dye from aqueous solution using single-wall carbon nanotubes: kinetic and equilibrium, *Desal. Wat. Treat.*, 51 (2013) 6507–6516.
- [55] N.F. Cardoso, E.C. Lima, B. Royer, M.V. Bach, G.L. Dotto, L.A.A. Pinto, T. Calvete, Comparison of *Spirulina platensis* microalgae and commercial activated carbon as adsorbents for the removal of Reactive Red 120 dye from aqueous effluents, *J. Hazard. Mater.*, 241–242 (2012) 146–153.

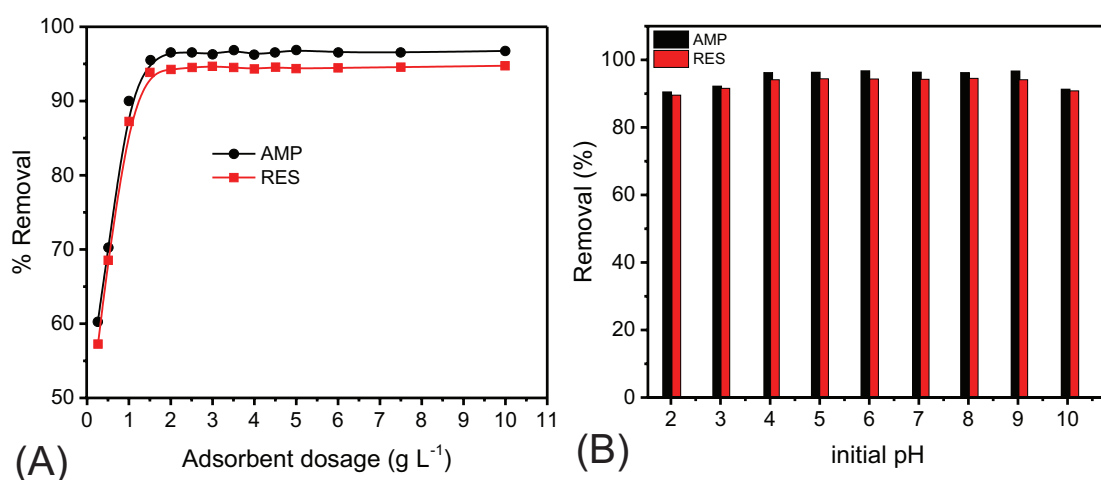
Supplementary information



Supplementary Fig. 1. (A) Structural formula of RES; pK_a values are expressed in the molecule. (B) Optimized three-dimensional structural formula of RES. The dimensions of the chemical molecule were calculated using MarvinSketch Version 16.6.6.0. Van der Waals surface area 158.58 Å² (pH 4.4–9.9); polar surface area 40.46 Å² (pH 0–9.1); dipole moment 0.33 Debye; logP 1.37; Davies hydrophilic–lipophilic balance (HLB) = 7.95.



Supplementary Fig. 2. (A) Structural formula of AMP; pK_a values are expressed in the molecule. (B) Optimized three-dimensional structural formula of AMP. The dimensions of the chemical molecule were calculated using MarvinSketch Version 16.6.6.0. Van der Waals surface area 161.92 Å² (pH 4.4–9.9); polar surface area 46.25 Å² (pH 4.4–9.9); dipole moment 4.09 Debye; logP 0.84; Davies hydrophilic–lipophilic balance (HLB) = 6.05.



Supplementary Fig. 3. (A) Effect of ASAC dosage and (B) effect of initial pH, on the adsorption of AMP and RES onto ASAC activated carbon. Conditions of (A): 300 mg L⁻¹ AMP and RES, 25°C, pH 6.0. Conditions of (B): 300 mg L⁻¹ AMP and RES, 25°C, adsorbent dosage 1.50 g L⁻¹.